THE JOURNAL OF PHYSICAL CHEMISTRY Letters

Letter

Cite This: J. Phys. Chem. Lett. 2019, 10, 6762−6770

pubs.acs.org/JPCL

Orbital Entanglement Analysis of Exchange-Coupled Systems

Christopher J. Stein,*,†,∥ Dimitrios A. Pantazis,*,‡ and Vera Krewald*,§

†Department of Chemistry, University of California, Berkeley, California 94720, United States

∥Chemical Sciences Division, Lawrence Berkeley National Laboratory, Berkeley, California 94720, United States

‡Max-Planck-Institut für Kohlenforschung, Kaiser-Wilhelm-Platz 1, 45470 Mülheim an der Ruhr, Germany

§Technische Universität Darmstadt, Fachbereich Chemie, Theoretische Chemie, Alarich-Weiss-Str. 4, 64287 Darmstadt, Germany

Supporting Information

ABSTRACT: A new tool for the interpretation of multiconfigurational wave functions representing the spin states of exchange-coupled transition metal complexes is introduced. Based on orbital entanglement measures, herein derived from multiconfigurational density matrix renormalization group calculations, the complexity of the wave function is reduced, thus facilitating a connection with established concepts for the interpretation of magnetically coupled systems. We show that the entanglement of localized orbitals with a small basis set is a good representation of the magnetic coupling topology and that it is sensitive to chemical changes in homologous complexes. Furthermore, we introduce a measure for the magnetic relevance of orbitals in the active subspace and a concept for the quantitative comparison of different chemical species. The approach presented here will be easily applicable to higher nuclearity clusters, providing a direct insight into all states of the Heisenberg spin ladder for systems previously accessible only by single-configurational methods.

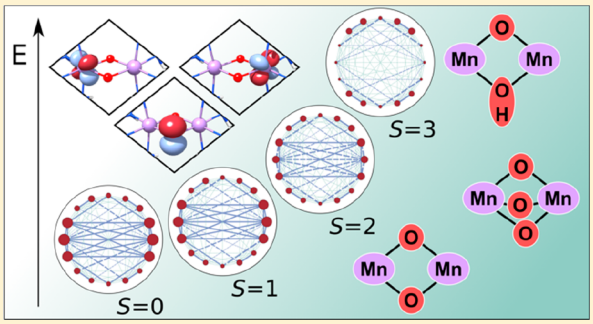

Due to their inherent complexity, multiconfigurational wave functions are often difficult to interpret. In contrast to single-determinant wave functions that can be directly associated with molecular orbital diagrams and electronic configurations, the analysis of such wave functions requires some form of information compression. In recent years, orbital entanglement has proven a versatile tool to achieve this goal.[1,2] Orbital entanglement is mostly discussed in the form of two quantities:[3] the single-orbital entropy $s_i(1)$ and the mutual information matrix $\boldsymbol{I}$, which in turn is calculated from $s_i(1)$ and a third quantity, the two-orbital entropy $s_{ij}(2)$. The single-orbital entropy is defined as

$$s_i(1) = -\sum_{\alpha=1}^{4} \omega_{\alpha,i} \ln \omega_{\alpha,i} \tag{1}$$

where α is the occupation of a spatial orbital (unoccupied, spin-up, spin-down, doubly occupied) and $\omega_{\alpha,i}$ is the eigenvalue of the reduced one-orbital density matrix. This Shannon-type entropy expression measures the deviation from a well-defined (or pure) occupation of orbital i in the multiconfigurational wave function and quantifies how much the occupation of a given orbital is influenced by the presence of all other orbitals.

The two-orbital entropy

$$s_{ij}(2) = -\sum_{\alpha=1}^{16} \omega_{\alpha,ij} \ln \omega_{\alpha,ij} \tag{2}$$

quantifies the uncertainty of the occupation defined for a pair of orbitals and is calculated from the eigenvalues of the two-orbital density matrix $\omega_{\alpha,ij}$. These two quantities can be combined to give the mutual information

$$\boldsymbol{I}_{ij} = \frac{1}{2}[s_i(1) + s_j(1) - s_{ij}(2)](1 - \delta_{ij}) \tag{3}$$

which quantifies the information loss on a pure orbital occupation for each individual orbital pair in the wave function. Because these entropy measures are calculated from the optimized multiconfigurational wave function, they strongly depend on both the spin state and the underlying molecular orbital basis.

Orbital entanglement has become popular in conjunction with the density matrix renormalization group (DMRG)[4−15] but can in principle be calculated from any multiconfigurational wave function.[16,17] DMRG, however, offers the added benefit of allowing access to large active spaces and will be the multiconfigurational solver in this Letter. Recent applications involving orbital entanglement in conjunction with DMRG include an optimized orbital ordering based on graph theory,[1] automated selection of active orbital spaces,[18,19] and analyses of chemical bonds.[20]

Received: August 17, 2019
Accepted: October 15, 2019
Published: October 15, 2019

DOI: 10.1021/acs.jpclett.9b02417
J. Phys. Chem. Lett. 2019, 10, 6762−6770

One prominent example for a problem with intrinsic multiconfigurational character is exchange coupling in oligonuclear transition metal complexes. The magnetic coupling in a system is often interpreted with magneto-structural correlations, which connect empirically known parameters, such as the types of bridge or metal−bridge−metal angles, with the detected magnetic behavior through the concepts of direct exchange and superexchange.[21−26] These correlations can often be linked straightforwardly to the results of single-configurational calculations such as broken-symmetry density functional theory (BS-DFT),[27−30] for instance, through the corresponding orbitals transformation.[31,32] This approach is generally applicable to two-spin-site systems but is of limited utility for oligonuclear systems with more complex bridging patterns.[26,33] BS-DFT has become an unrivaled tool for the interpretation of magnetic experiments due to its wide applicability, high accuracy if calibrated correctly, and ease of use. Disadvantages of BS-DFT include its inability to describe all individual spin states of the Heisenberg ladder and its lack of systematic improvability.[34] *Ab initio* calculations on magnetically coupled systems have been carried out with difference-dedicated configuration interaction (DDCI) and complete active space methods (CASSCF/CASPT2) among others, including an analysis of the underlying physics.[35−44] With the impending facile accessibility of multiconfigurational descriptions for many oligonuclear systems with DMRG,[45−49] analytical tools are needed that connect the quantum-chemical description to established interpretations and chemical concepts. Other efforts in this direction are based on a Green's-function approach that also allows a fragment-based analysis.[50,51]

Herein, we show how orbital entanglement measures can be connected to the magnetic topology of an exchange-coupled system represented by a multiconfigurational wave function, and demonstrate how changes in magnetic pathways due to chemical modifications in homologous complexes can be revealed and quantitatively analyzed. We note that for a numerically accurate reproduction of the exchange coupling constant itself, subsequent perturbation theory treatment as described earlier is needed to recover dynamical correlation, but the predicted coupling topology will not be affected by this.[46]

Given that Mn-oxo dimers are particularly well understood and the orbitals that need to be included in the active space are clear from magnetostructural correlations and prior studies,[52−58] they represent an ideal test case for such an analysis that aims at a detailed understanding of the importance of individual bridges to the magnetic coupling. The key geometric features of three representative dimers and the coupling constants predicted with BS-DFT are shown in Figure 1.

As long as all orbitals constituting the multiconfigurational problem (e.g., the whole valence space) are included in the wave function, any unitary transformation of this active orbital subspace is valid. Given this freedom, we can choose an orbital basis that best aligns with an intuitive chemical picture. In the case of magnetic coupling, these are the metal-centered magnetic orbitals and orbitals centered on the bridging ligands, which can be generated by localization schemes. For the present Letter, we sequentially apply the Pipek−Mezey localization procedure to the doubly occupied, singly occupied, and virtual orbital subspaces of the minimal basis high-spin Hartree−Fock solution. From those, we select the bonding and antibonding Mn−O σ-orbitals, noninteracting O p_z orbitals,

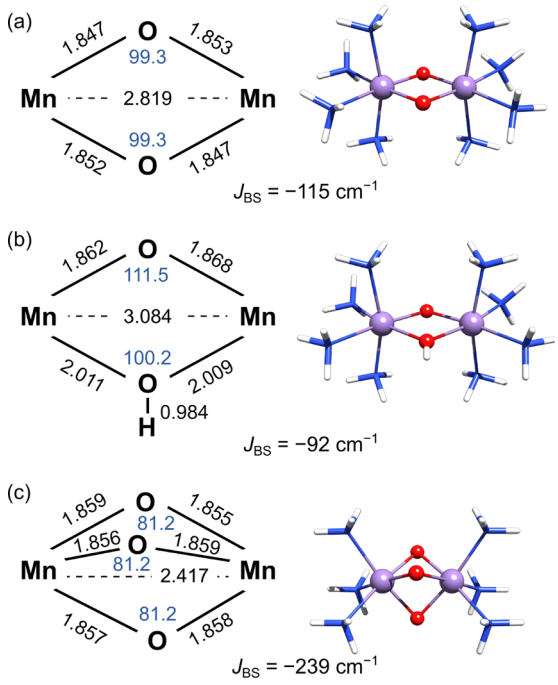

Figure 1. Key geometric features of the three Mn(IV) model dimers and the coupling constant J_{BS} (cm^{-1}) derived in ref 56 from BS-DFT with the TPSSh density functional. Distances are given in Å (black), angles in degrees (blue). (a) $[Mn(IV)_2(\mu\text{-}O)_2(NH_3)_8]^{4+}$, (b) $[Mn(IV)_2(\mu\text{-}O)(\mu\text{-}OH)(NH_3)_8]^{5+}$, (c) $[Mn(IV)_2(\mu\text{-}O)_3(NH_3)_6]^{2+}$.

and magnetic Mn 3d orbitals as an active orbital space for multiconfigurational calculations (see Figures 2a and S1). For the Mn_2O_2 core, the multiconfigurational problem is thus defined by 16 orbitals (Figure S2 shows that the O 2s orbitals are not relevant).

A straightforward graphical representation of the orbital entanglement measures introduced above are entanglement diagrams (see Figure 2), where all active orbitals are arranged on a circle and the single-orbital entropy is proportional to the radius of a red circle associated with each orbital. The thickness of lines connecting these circles is proportional to the mutual information element for each pair of orbitals. In the entanglement diagram of the singlet state (Figure 2a, top), six orbitals stand out: they have the largest single orbital entropies, and all possible pairs are interconnected by a large mutual information element. These are the magnetic orbitals, d(x^2-y^2) and linear combinations of d(xz) and d(yz) oriented along the Mn−O bonds. The mutual information on the latter with the O p_z orbitals they are oriented toward is almost as strong as among the magnetic orbitals themselves, whereas there is no significant mutual information connecting the O p_z with the remaining magnetic orbitals. This representation is congruent with the empirical picture of superexchange mediated by bridging ligands. In the orbital basis shown in Figure 2, the other O p orbitals are part of σ/σ^* pairs. Their mutual information element is strongest among themselves and, in fact, an order of magnitude larger than with any of the magnetic orbitals. No significant mutual information is found for the O p_z orbitals and the σ/σ^* pairs.

For the magnetically less coupled states of the Heisenberg spin ladder (Figure 2a, bottom), the mutual information and the single orbital entropies of the magnetic and O p_z orbitals are significantly decreased. In contrast, the entanglement of the

DOI: 10.1021/acs.jpclett.9b02417
J. Phys. Chem. Lett. 2019, 10, 6762−6770

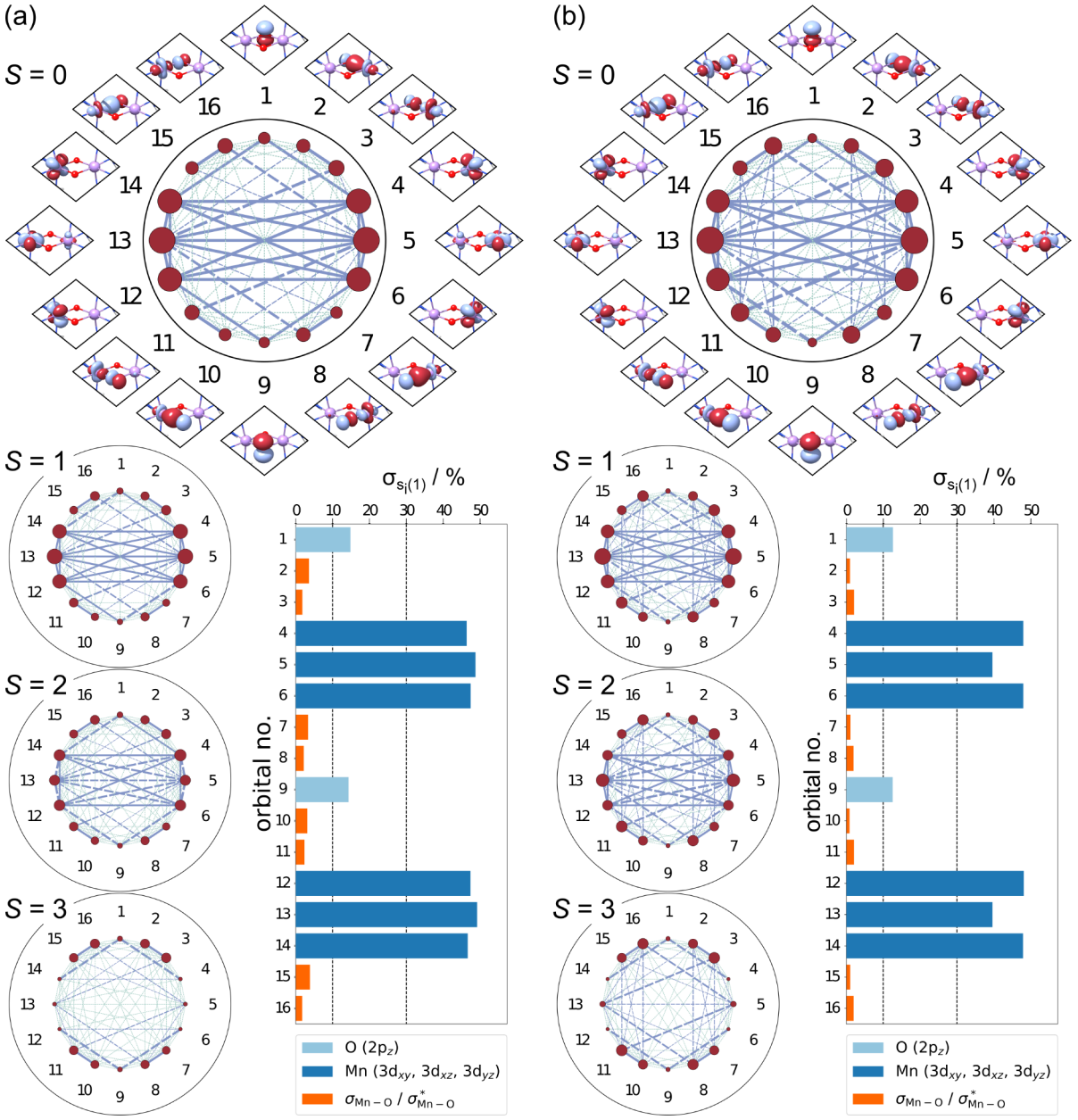

Figure 2. Orbital entanglement diagrams of bis-μ-oxo-bridged dimer in the singlet, triplet, and septet states based on (a) localized orbitals (DMRG-CI) with a small basis and (b) optimized orbitals (DMRG-SCF) with a larger triple-ζ basis. The bar diagrams show the relative standard deviation of the single orbital entropy across all spin states.

σ/σ^* pairs remains unchanged. In the high spin (septet) state, the only other relevant entanglement remaining is that of the O p_z and the corresponding d-orbital at each Mn ion. Hence, the entanglement of the magnetic and O p_z orbitals is strongly spin dependent, which leads us to conclude that only these orbitals are relevant for the description of exchange coupling. We emphasize that the single-orbital entropy contains much more information than the orbital occupation numbers. While the occupation numbers of the magnetic orbitals are close to 1 for all spin states (Table S22), the single-orbital entropy captures the fact that in the low spin states these electrons are spin up in some determinants, whereas they are spin down in others due to the antiferromagnetic coupling. The single-orbital entropy is hence capable of reflecting their magnetic relevance, whereas this is not the case for the occupation numbers. As a quantitative measure for the spin-state dependency of the entanglement, we calculate the relative standard deviation of the single orbital entropy over all spin states (bar diagram in Figure 2a; see Table S1 for absolute values and Tables S2−S5 for mutual information matrices). The most pronounced change is observed for the magnetic orbitals, where the relative standard deviation reaches almost 50%. For the O p_z orbitals, the change amounts to ca. 15% and is thus much more significant than for the σ/σ^* pairs (<5%). The relative standard deviation of the single orbital entropy allows us to rank the importance of orbitals in the active subspace and will subsequently be referred to as the magnetic relevance. We note that this result—the spin state of the system dominantly affecting pseudoatomic orbitals that can interact in π/π^* fashion—aligns perfectly with the chemical concept of π-exchange pathways.

DOI: 10.1021/acs.jpclett.9b02417
J. Phys. Chem. Lett. 2019, 10, 6762−6770

So far, localized orbitals in a small basis have been used. Upon optimizing the orbitals for each spin state with DMRG-SCF and a triple-ζ atomic orbital basis set, neither a qualitative nor a quantitative change can be observed in the entanglement measures (Figure 2b, see also Tables S6−S10). This shows that for the present complex, the localized orbital basis is already very close to the converged basis and highlights the locality of the multiconfigurational problem. We observe that for all systems studied herein a small, localized basis set is adequate to obtain a qualitative insight into the magnetic coupling. A projection of the localized orbitals onto a larger basis set and subsequent state-specific optimization shows no qualitative changes (see Figures S3 and S4). This is also reflected in the unchanged orbital occupation numbers (max. deviation: 0.04 for the oxygen p_z orbitals in the singlet state). The effect of adding a so-called double shell was investigated, and the 4d orbitals are not entangled to a significant extent (see Figure S12). Adding a double d shell is important for late transition metals to recover correlation, but these orbitals are not expected to be important for a qualitative representation of the coupling topology—or in other words, they do not act as acceptor orbitals in the types of charge-transfer excitation that describe the fundamental physics involved in magnetic coupling.[42]

To be useful in the analysis of exchange coupling pathways, it is a fundamental requirement for a method to be able to discriminate between different types of bridging ligand. Therefore, we investigate if and how the entanglement analysis differs for the singly protonated analogue of the bis-μ-oxo core: the μ-oxo-μ-hydroxo-bridged Mn(IV) dimer. According to BS-DFT calculations, the coupling strength decreases from −115 to −92 cm^{-1} upon protonation,[56] a smaller decrease than observed experimentally upon single protonation of salpn-ligated Mn(IV) dimers (exptl, −92 to −48 cm^{-1}; calcd crystal structure −101 to −46 cm^{-1}).[59,58] The reason for this decrease was postulated to originate from shutting down certain exchange-coupling pathways. The entanglement of the respective orbitals offers a direct way to evaluate this assumption.

Indeed, protonation leads to a very small entanglement of the σ/σ^* orbitals involving the hydroxo bridge and of the OH-centered p_z orbital with the magnetic orbitals (Figures 3 and S5), implying that the hydroxo bridge does not participate in superexchange. In contrast, the entanglement of the oxo bridge remains unchanged with respect to the Mn_2O_2 core (see Tables S11−S15 for exact values). This observation holds true for all spin states and thus aligns with the empirically deduced picture of the deactivated pathway. The magnetic relevance of the OH p_z orbital is lowered to ca. 7%, i.e., only slightly larger than any of the σ/σ^* pairs (Figure 3, bar diagram). It is important to note that in the ammonia-saturated model system studied here, protonation leads to more pronounced structural changes than in synthetically accessible complexes: an increase in Mn−Mn distance by ca. 0.1 Å (salpn) vs ca. 0.3 Å (NH_3), and an increase in Mn−O−Mn angle by ca. 7° (salpn) vs 12° (NH_3). For the present system, we can therefore not firmly say whether the increase in magnetic relevance of the O p_z and magnetic orbitals upon protonation is dominated by electronic or structural differences within the Mn_2O_2 core.

For the orbital optimization, the weakly entangled O p_z orbital on the hydroxo bridge is excluded (Figures S6−S8; see also Tables S16−S20). No qualitative change is observed, confirming that the localized orbitals with a small basis set are

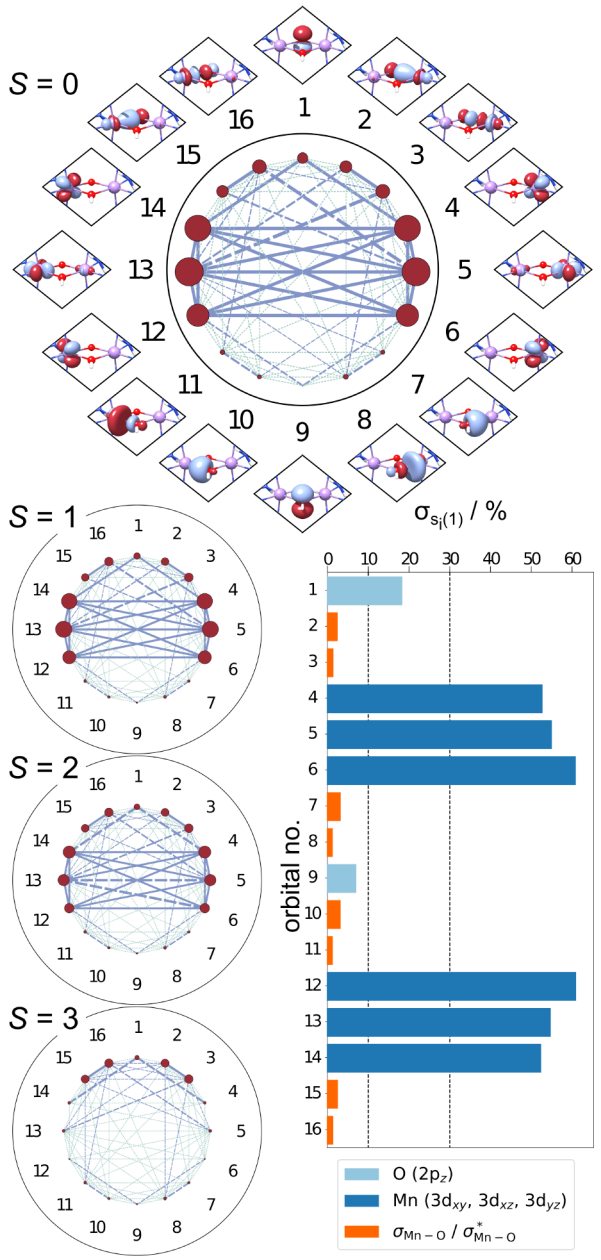

Figure 3. Orbital entanglement diagrams for the μ-oxo-μ-hydroxo-bridged dimer in all spin states based on localized orbitals (DMRG-CI) with a small basis set, including a bar diagram of the relative standard deviation of the single orbital entropy across all spin states.

yet again a good qualitative approximation to the fully optimized large basis set in which the multiconfigurational problem is solved.

The above cases establish that entanglement analysis can provide a picture of superexchange coupling pathways that accurately identifies the role of chemically different bridging ligands in accordance with experimentally known facts. An important structural parameter pertaining to superexchange paths is the metal−bridge−metal angle. We therefore studied a tris-μ-oxo bridged Mn(IV) dimer with significantly more acute angles (see Figure 1), the synthetic analogue of which shows an exceptionally strong coupling constant (−390 cm^{-1}).[60] The origin of this strong coupling has been attributed to direct exchange contributions alongside superexchange pathways.[56,61] As in the previous examples, the magnetic orbitals stand out in

DOI: 10.1021/acs.jpclett.9b02417
J. Phys. Chem. Lett. 2019, 10, 6762−6770

the entanglement diagrams because of their large single-orbital entropy and the fact that they are all connected by large mutual information elements (Figures 4 and S9–S11). The O p_z orbitals, however, despite still being connected to a magnetic orbital on each manganese ion via a large mutual information element, show a reduced single-orbital entropy when compared to the μ-oxo bridges in the examples above. This is likely the result of a reduced overlap of the O p_z and magnetic orbitals due to the acute Mn–O–Mn angles in the tris-μ-oxo core. An analysis of the magnetic relevance, however, shows a similar picture as in the case of the Mn_2O_2 model compound: the magnetic, O p_z and σ/σ^* orbitals group by decreasing spin-dependence of the single-orbital entropy. Again, the qualitative analysis based on localized orbitals with a small basis is practically identical to the results from optimized orbitals with a large basis set (Tables S21–S30 and Figures S9–S10).

So far, we have shown that orbital entanglement can serve as an analysis tool for exchange coupling topologies and yields an intuitive picture that aligns with empirical concepts for the interpretation of magnetic interactions. Since the mutual information measures to what extent each orbital within a pair of orbitals influences the occupation of the other, we expect different contributions to magnetic coupling to be reflected in the mutual information sums calculated for groups of orbitals reflecting the topology. For a comparative and quantitative analysis of the individual contributors across different complexes, we calculate the sum of mutual information elements connecting particular orbital sets in the singlet state: the three magnetic orbitals on each manganese ion (i.e., two sets of three orbitals each) and the O p_z orbital (two or three sets of one orbital each, see Figure 5).

All mutual information sums confirm that the same exchange coupling picture emerges with localized (blue numbers in Figure 5) and optimized (black numbers in Figure 5) orbitals. Taking the bis-μ-oxo-bridged complex as a reference (Figure 5a), it is clear that the coupling pathway involving the hydroxo bridge is switched off (Figure 5b), whereas the mutual

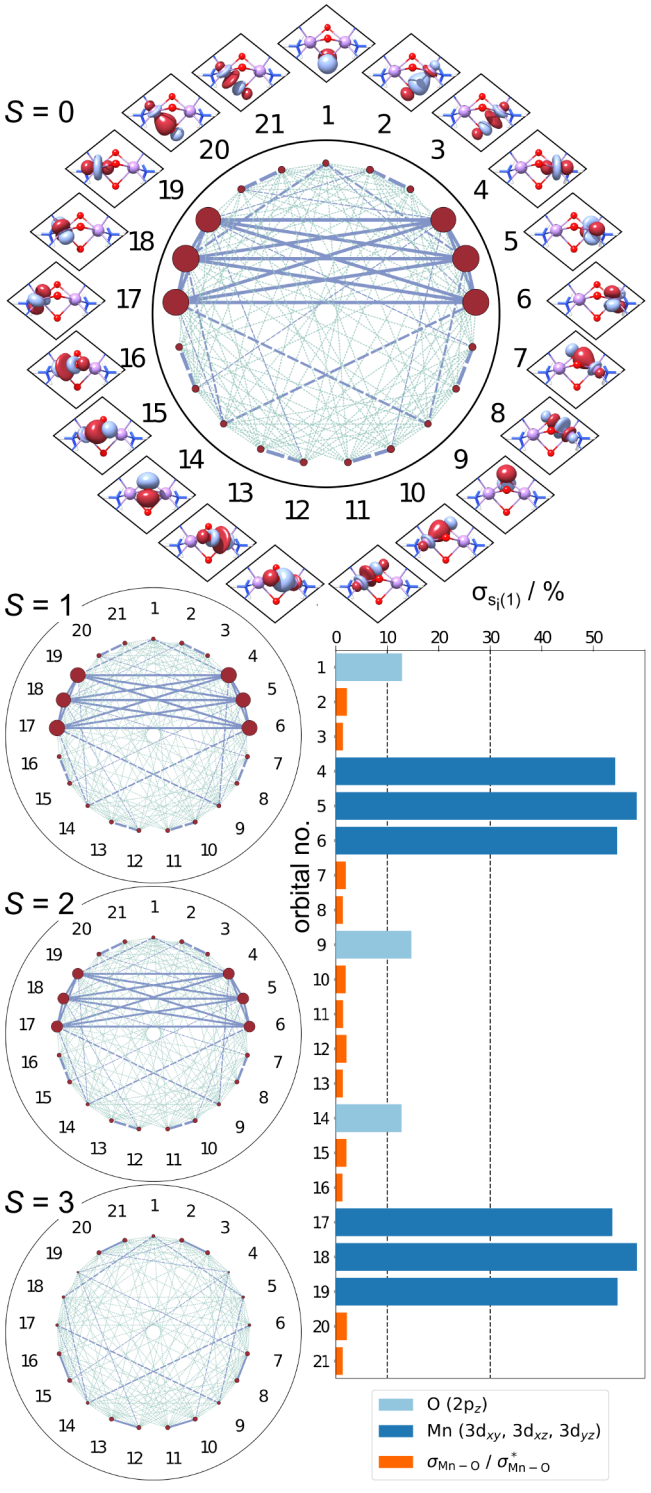

Figure 4. Orbital entanglement diagrams for the tris-μ-oxo-bridged dimer in all spin states based on (a) localized orbitals (DMRG-CI) with a small basis set, including a bar diagram of the relative standard deviation of the single orbital entropy across all spin states.

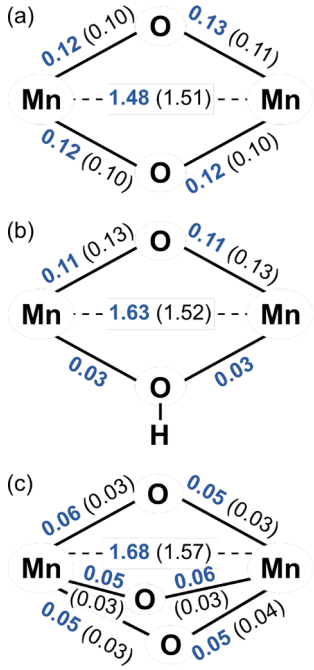

Figure 5. Quantitative analysis of magnetic coupling with the sum of mutual information elements for the most relevant orbital classes, the magnetic orbitals on each manganese ion, and the O p_z orbitals of the oxo bridges. Bold blue numbers are from the DMRG-CI localized orbital basis, and black numbers in parentheses are from the DMRG-SCF optimized orbital basis.

DOI: 10.1021/acs.jpclett.9b02417
J. Phys. Chem. Lett. 2019, 10, 6762–6770

information sum involving the magnetic orbitals is slightly increased in the case of the localized orbitals. We note that the values for the optimized orbital basis associated with the oxo-bridge in the protonated dimer are larger than in the bis-μ-oxo example. While this observation is in qualitative agreement with the magnitude of the exchange coupling pathway not being halved (-115 cm^{-1} vs -92 cm^{-1}), a quantitative analysis also taking into account the structural changes induced upon protonation will require a more extensive investigation. The mutual information sums for the oxo bridges in the tris-μ-oxo case are distinctly smaller than for the oxo bridges in the other two examples, an effect that is more pronounced in the optimized orbital basis (Figure 5c). Whether this can be attributed to geometric effects due to the acute angle at the oxo-bridges (Mn−O−Mn: ca. 81°), the shorter Mn−Mn distance (2.82 Å in bis-μ-oxo vs 2.41 Å in tris-μ-oxo), and/or dominant direct exchange effects can presently not be ascertained.

CONCLUSIONS

We introduced a new type of analysis for magnetically coupled systems based on orbital entanglement. We demonstrated that DMRG-CI wave functions calculated in a localized orbital basis constructed from a minimal atomic-orbital basis set are adequate for an assessment of electronic structure differences across all spin states of the Heisenberg ladder. Optimization of these orbitals in a larger basis set affords an identical interpretation. The entanglement diagrams readily show which pathways are involved in the coupling. We introduce the relative standard deviation of the single orbital entropy across all spin states as the magnetic relevance of the respective orbitals, i.e., their importance for the magnetic coupling topology.

Our concept opens the possibility to investigate oligonuclear systems that have active spaces for which orbital optimization may not be easy. Given that DMRG-CI is presently feasible for up to (40,40) active spaces,[62] our analysis can target systems previously accessible only by BS-DFT, for instance, the valence active space of tetranuclear clusters with up to six bridges or the valence active space plus a metal double d-shell for trinuclear clusters with three bridging atoms. The orbital entanglement analysis of exchange-coupled systems is applicable to all individual spin states of the Heisenberg ladder and can thus be viewed as complementary as well as supplementary to a BS-DFT analysis, in particular for systems with more than two magnetic centers. Furthermore, our approach permits the individual assessment of particular elements of the magnetic coupling topology, for instance, the contributions of specific bridges or so-called "double shell" effects, without the need for orbital optimization. In line with the orbital entanglement based automated active space selection,[18,19] for complicated coupling topologies, such an analysis would identify the ideal active space for a quantitative calculation of the coupling constant magnitude. The latter would then be calculated with a large atomic-orbital basis set, multispin state-averaging for the orbital optimization, and subsequent perturbation theory treatment.[46,48]

Computational Details. The coordinates for the three dimers were taken from ref 56. All calculations were performed with OpenMolcas[62] and an interface to the QCMaquis DMRG program.[63,64] The two basis sets were ANO-RCC-MB on all atoms, or ANO-RCC-VTZP for Mn and O and ANO-RCC-VDZP on N and H.[65,66] Scalar-relativistic effects were included to second order by means of the Douglas−Kroll−Hess Hamiltonian,[67−69] and the localized orbitals were obtained with the Pipek−Mezey localization scheme.[70] In the DMRG calculations, the maximum bond dimension was set to 1000, and the number of sweeps was set to 20. Note that the entanglement information converges much faster than the energy. The convergence with respect to the maximum bond dimension m was analyzed (Figure S13), and no meaningful improvement was found for m = 2000 over m = 1000 such that the latter was chosen in order to reduce the computational cost. We use standard orbital ordering procedures according to the default settings of the QCMaquis DMRG program.[14,63] The orbital ordering was unaltered, meaning that it corresponds to the results of the localization procedure with doubly occupied orbitals at the beginning of the DMRG lattice, followed by the singly occupied magnetic orbitals and the unoccupied orbitals. Note that the entanglement diagrams show a manipulated ordering that reflects the topology of the complexes studied here. The initial guess for the matrix product state (MPS) wave function was also obtained from the default option in QCMaquis that employs random numbers but generates an MPS structure with proper dimensionality on each site. We emphasize that these standard settings may need to be optimized for strongly correlated systems, where a CI-DEAS initial guess[1,71] and an orbital ordering according to the Fiedler vector[72,73] is likely to substantially improve the convergence. The orbital entanglement information on these DMRG calculations was analyzed with the autoCAS program,[74] which also provided the entanglement diagrams. Orbital optimizations were carried out as state-specific optimizations where indicated in the main text. Since purely hypothetical model complexes are used, the aim of the calculations is not the extraction of the exchange coupling constant J but a representation of all spin states of the spin ladder.

ASSOCIATED CONTENT

Supporting Information

The Supporting Information is available free of charge on the ACS Publications website at DOI: 10.1021/acs.jpclett.9b02417.

Pictures of active space and additional orbitals; additional entanglement diagrams; single orbital entropies, magnetic relevance, and mutual information matrices for all dimers with large and small basis sets (PDF)

AUTHOR INFORMATION

Corresponding Authors

*E-mail: cjstein@lbl.gov.
*E-mail: dimitrios.pantazis@kofo.mpg.de.
*E-mail: krewald@chemie.tu-darmstadt.de.

ORCID

Dimitrios A. Pantazis: 0000-0002-2146-9065
Vera Krewald: 0000-0002-4749-4357

Notes

The authors declare no competing financial interest.

ACKNOWLEDGMENTS

C.J.S. gratefully acknowledges financial support in the form of an *Early Postdoc.Mobility* fellowship from the Swiss National Science Foundation. D.A.P. acknowledges the Max Planck

DOI: 10.1021/acs.jpclett.9b02417
J. Phys. Chem. Lett. 2019, 10, 6762−6770

Society for financial support. Extensive calculations on the Lichtenberg high-performance computer of the Technische Universität Darmstadt were conducted for this work. The authors thank the Hessian Competence Center for High Performance Computing—funded by the Hessen State Ministry of Higher Education, Research and the Arts—for helpful advice.

REFERENCES

(1) Legeza, O.; Solyom, J. Optimizing the density-matrix renormalization group method using quantum information entropy. *Phys. Rev. B: Condens. Matter Mater. Phys.* **2003**, *68* (19), 195116.
(2) Rissler, J.; Noack, R. M.; White, S. R. Measuring orbital interaction using quantum information theory. *Chem. Phys.* **2006**, *323* (2−3), 519−531.
(3) Boguslawski, K.; Tecmer, P.; Barcza, G.; Legeza, O.; Reiher, M. Orbital Entanglement in Bond-Formation Processes. *J. Chem. Theory Comput.* **2013**, *9* (7), 2959−2973.
(4) White, S. R. Density matrix formulation for quantum renormalization groups. *Phys. Rev. Lett.* **1992**, *69* (19), 2863−2866.
(5) White, S. R. Density-matrix algorithms for quantum renormalization groups. *Phys. Rev. B: Condens. Matter Mater. Phys.* **1993**, *48* (14), 10345−10356.
(6) Chan, G. K.-L.; Zgid, D. The Density Matrix Renormalization Group in Quantum Chemistry. In *Annual Reports in Computational Chemistry*; Elsevier, 2009; Vol. *5*, Chapter 7, pp 149−162.
(7) Marti, K. H.; Reiher, M. The Density Matrix Renormalization Group Algorithm in Quantum Chemistry. *Z. Phys. Chem.* **2010**, *224* (3−4), 583−599.
(8) Schollwöck, U. The density-matrix renormalization group in the age of matrix product states. *Ann. Phys.* **2011**, *326* (1), 96−192.
(9) Chan, G. K.; Sharma, S. The density matrix renormalization group in quantum chemistry. *Annu. Rev. Phys. Chem.* **2011**, *62*, 465−481.
(10) Marti, K. H.; Reiher, M. New electron correlation theories for transition metal chemistry. *Phys. Chem. Chem. Phys.* **2011**, *13* (15), 6750−9.
(11) Kurashige, Y. Multireference electron correlation methods with density matrix renormalisation group reference functions. *Mol. Phys.* **2014**, *112* (11), 1485−1494.
(12) Wouters, S.; Van Neck, D. The density matrix renormalization group for ab initio quantum chemistry. *Eur. Phys. J. D* **2014**, *68* (9), 272.
(13) Szalay, S.; Pfeffer, M.; Murg, V.; Barcza, G.; Verstraete, F.; Schneider, R.; Legeza, Ö. Tensor product methods and entanglement optimization for ab initio quantum chemistry. *Int. J. Quantum Chem.* **2015**, *115* (19), 1342−1391.
(14) Knecht, S.; Hedegard, E. D.; Keller, S.; Kovyrshin, A.; Ma, Y.; Muolo, A.; Stein, C. J.; Reiher, M. New Approaches for ab initio Calculations of Molecules with Strong Electron Correlation. *Chimia* **2016**, *70* (4), 244−51.
(15) Chan, G. K.; Keselman, A.; Nakatani, N.; Li, Z.; White, S. R. Matrix product operators, matrix product states, and ab initio density matrix renormalization group algorithms. *J. Chem. Phys.* **2016**, *145* (1), 014102.
(16) Boguslawski, K.; Tecmer, P. Orbital entanglement in quantum chemistry. *Int. J. Quantum Chem.* **2015**, *115* (19), 1289−1295.
(17) Boguslawski, K.; Tecmer, P.; Legeza, Ö. Analysis of two-orbital correlations in wave functions restricted to electron-pair states. *Phys. Rev. B: Condens. Matter Mater. Phys.* **2016**, *94* (15), 155126.
(18) Stein, C. J.; Reiher, M. Automated Selection of Active Orbital Spaces. *J. Chem. Theory Comput.* **2016**, *12* (4), 1760−1771.
(19) Stein, C. J.; Reiher, M. Automated Identification of Relevant Frontier Orbitals for Chemical Compounds and Processes. *Chimia* **2017**, *71* (4), 170−176.
(20) Szalay, S.; Barcza, G.; Szilvasi, T.; Veis, L.; Legeza, O. The correlation theory of the chemical bond. *Sci. Rep.* **2017**, *7* (1), 2237.
(21) Anderson, P. W. Antiferromagnetism. Theory of Superexchange Interaction. *Phys. Rev.* **1950**, *79* (2), 350−356.
(22) Goodenough, J. B. Theory of the Role of Covalence in the Perovskite-Type Manganites [La, M(II)]MnO_3. *Phys. Rev.* **1955**, *100* (2), 564−573.
(23) Anderson, P. W. New Approach to the Theory of Superexchange Interactions. *Phys. Rev.* **1959**, *115* (1), 2−13.
(24) Kanamori, J. Superexchange interaction and symmetry properties of electron orbitals. *J. Phys. Chem. Solids* **1959**, *10* (2), 87−98.
(25) Hay, P. J.; Thibeault, J. C.; Hoffmann, R. Orbital interactions in metal dimer complexes. *J. Am. Chem. Soc.* **1975**, *97* (17), 4884−4899.
(26) Bencini, A.; Gatteschi, D. Angular overlap interpretation of the magnetic properties of copper(II) dimers. *Inorg. Chim. Acta* **1978**, *31*, 11−18.
(27) Noodleman, L. Valence bond description of anti-ferromagnetic coupling in transition-metal dimers. *J. Chem. Phys.* **1981**, *74*, 5737−5743.
(28) Noodleman, L.; Peng, C. Y.; Case, D. A.; Mouesca, J. M. Orbital interactions, electron delocalization and spin coupling in iron-sulfur clusters. *Coord. Chem. Rev.* **1995**, *144*, 199−244.
(29) Caballol, R.; Castell, O.; Illas, F.; de P. R. Moreira, I.; Malrieu, J. P. Remarks on the Proper Use of the Broken Symmetry Approach to Magnetic Coupling. *J. Phys. Chem. A* **1997**, *101* (42), 7860−7866.
(30) Ruiz, E.; Cano, J.; Alvarez, S.; Alemany, P. Broken symmetry approach to calculation of exchange coupling constants for homobinuclear and heterobinuclear transition metal complexes. *J. Comput. Chem.* **1999**, *20*, 1391−1400.
(31) Amos, A. T.; Hall, G. G. Single Determinant Wave Functions. *Proc. R. Soc. London, A* **1961**, *263* (131), 483−493.
(32) Neese, F. Definition of corresponding orbitals and the diradical character in broken symmetry DFT calculations on spin coupled systems. *J. Phys. Chem. Solids* **2004**, *65*, 781−785.
(33) Krewald, V.; Neese, F.; Pantazis, D. A. On the Magnetic and Spectroscopic Properties of High-Valent Mn_3CaO_4 Cubanes as Structural Units of Natural and Artificial Water-Oxidizing Catalysts. *J. Am. Chem. Soc.* **2013**, *135* (15), 5726−5739.
(34) Orio, M.; Pantazis, D. A.; Petrenko, T.; Neese, F. Magnetic and Spectroscopic Properties of Mixed Valence Manganese(III,IV) Dimers: A Systematic Study Using Broken Symmetry Density Functional Theory. *Inorg. Chem.* **2009**, *48* (15), 7251−7260.
(35) De Loth, P.; Cassoux, P.; Daudey, J. P.; Malrieu, J. P. Ab initio direct calculation of the singlet-triplet separation in cupric acetate hydrate dimer. *J. Am. Chem. Soc.* **1981**, *103* (14), 4007−4016.
(36) de Graaf, C.; Sousa, C.; de, P. R.; Moreira, I.; Illas, F. Multiconfigurational Perturbation Theory: An Efficient Tool to Predict Magnetic Coupling Parameters in Biradicals, Molecular Complexes, and Ionic Insulators. *J. Phys. Chem. A* **2001**, *105* (50), 11371−11378.
(37) Calzado, C. J.; Cabrero, J.; Malrieu, J. P.; Caballol, R. Analysis of the magnetic coupling in binuclear complexes. I. Physics of the coupling. *J. Chem. Phys.* **2002**, *116* (7), 2728−2747.
(38) Calzado, C. J.; Cabrero, J.; Malrieu, J. P.; Caballol, R. Analysis of the magnetic coupling in binuclear complexes. II. Derivation of valence effective Hamiltonians from ab initio CI and DFT calculations. *J. Chem. Phys.* **2002**, *116* (10), 3985−4000.
(39) Hubner, O.; Fink, K.; Klopper, W. The spin coupling in the diiron complex $[Fe_2(hpdta)(H_2O)_3Cl]$. *Phys. Chem. Chem. Phys.* **2007**, *9* (16), 1911−1920.
(40) Calzado, C. J.; Angeli, C.; Taratiel, D.; Caballol, R.; Malrieu, J.-P. Analysis of the magnetic coupling in binuclear systems. III. The role of the ligand to metal charge transfer excitations revisited. *J. Chem. Phys.* **2009**, *131* (4), 044327.
(41) Vogiatzis, K. D.; Klopper, W.; Mavrandonakis, A.; Fink, K. Magnetic properties of paddlewheels and trinuclear clusters with exposed metal sites. *ChemPhysChem* **2011**, *12*, 3307−3319.
(42) Malrieu, J. P.; Caballol, R.; Calzado, C. J.; de Graaf, C.; Guihéry, N. Magnetic Interactions in Molecules and Highly Correlated Materials: Physical Content, Analytical Derivation, and

DOI: 10.1021/acs.jpclett.9b02417
J. Phys. Chem. Lett. 2019, 10, 6762−6770

Rigorous Extraction of Magnetic Hamiltonians. *Chem. Rev.* **2014**, *114* (1), 429−492.
(43) Angeli, C.; Calzado, C. J. The role of the magnetic orbitals in the calculation of the magnetic coupling constants from multi-reference perturbation theory methods. *J. Chem. Phys.* **2012**, *137* (3), 034104.
(44) Tenti, L.; Maynau, D.; Angeli, C.; Calzado, C. J. Highly efficient perturbative + variational strategy based on orthogonal valence bond theory for the evaluation of magnetic coupling constants. Application to the trinuclear Cu(II) site of multicopper oxidases. *Phys. Chem. Chem. Phys.* **2016**, *18* (27), 18365−18380.
(45) Harris, T. V.; Kurashige, Y.; Yanai, T.; Morokuma, K. Ab initio density matrix renormalization group study of magnetic coupling in dinuclear iron and chromium complexes. *J. Chem. Phys.* **2014**, *140* (5), 054303.
(46) Roemelt, M.; Krewald, V.; Pantazis, D. A. Exchange Coupling Interactions from the Density Matrix Renormalization Group and N-Electron Valence Perturbation Theory: Application to a Biomimetic Mixed-Valence Manganese Complex. *J. Chem. Theory Comput.* **2018**, *14* (1), 166−179.
(47) Roemelt, M.; Pantazis, D. A. Multireference Approaches to Spin-State Energetics of Transition Metal Complexes Utilizing the Density Matrix Renormalization Group. *Adv. Theory Simul.* **2019**, *2* (5), 1800201.
(48) Krewald, V.; Pantazis, D. A. Applications of the Density Matrix Renormalization Group to Exchange-Coupled Transition Metal Systems. In *Transition Metals in Coordination Environments: Computational Chemistry and Catalysis Viewpoints*; Broclawik, E., Borowski, T., Radoń, M., Eds.; Springer International Publishing: Cham, Switzerland, 2019; pp 91−120.
(49) Pantazis, D. A. Meeting the Challenge of Magnetic Coupling in a Triply-Bridged Chromium Dimer: Complementary Broken-Symmetry Density Functional Theory and Multireference Density Matrix Renormalization Group Perspectives. *J. Chem. Theory Comput.* **2019**, *15* (2), 938−948.
(50) Steenbock, T.; Tasche, J.; Lichtenstein, A. I.; Herrmann, C. A Green's-Function Approach to Exchange Spin Coupling As a New Tool for Quantum Chemistry. *J. Chem. Theory Comput.* **2015**, *11* (12), 5651−5664.
(51) Steenbock, T.; Herrmann, C. Toward an automated analysis of exchange pathways in spin-coupled systems. *J. Comput. Chem.* **2018**, *39* (2), 81−92.
(52) Zhao, X. G.; Richardson, W. H.; Chen, J. L.; Li, J.; Noodleman, L.; Tsai, H. L.; Hendrickson, D. N. Density Functional Calculations of Electronic Structure, Charge Distribution, and Spin Coupling in Manganese-Oxo Dimer Complexes. *Inorg. Chem.* **1997**, *36* (6), 1198−1217.
(53) Mukhopadhyay, S.; Mandal, S. K.; Bhaduri, S.; Armstrong, W. H. Manganese clusters with relevance to photosystem II. *Chem. Rev.* **2004**, *104* (9), 3981−4026.
(54) Rudberg, E.; Sałek, P.; Rinkevicius, Z.; Ågren, H. Heisenberg Exchange in Dinuclear Manganese Complexes: A Density Functional Theory Study. *J. Chem. Theory Comput.* **2006**, *2* (4), 981−989.
(55) Pantazis, D. A.; Orio, M.; Petrenko, T.; Zein, S.; Bill, E.; Lubitz, W.; Messinger, J.; Neese, F. A new quantum chemical approach to the magnetic properties of oligonuclear transition-metal complexes: Application to a model for the tetranuclear manganese cluster of Photosystem II. *Chem. - Eur. J.* **2009**, *15* (20), 5108−5123.
(56) Pantazis, D. A.; Krewald, V.; Orio, M.; Neese, F. Theoretical magnetochemistry of dinuclear manganese complexes: broken symmetry density functional theory investigation on the influence of bridging motifs on structure and magnetism. *Dalton Trans.* **2010**, *39* (20), 4959−4967.
(57) Cox, N.; Ames, W.; Epel, B.; Kulik, L. V.; Rapatskiy, L.; Neese, F.; Messinger, J.; Wieghardt, K.; Lubitz, W. Electronic Structure of a Weakly Antiferromagnetically Coupled $Mn^{II}Mn^{III}$ Model Relevant to Manganese Proteins: A Combined EPR, ^{55}Mn-ENDOR, and DFT Study. *Inorg. Chem.* **2011**, *50* (17), 8238−8251.
(58) Krewald, V.; Lassalle-Kaiser, B.; Boron, T. T.; Pollock, C. J.; Kern, J.; Beckwith, M. A.; Yachandra, V. K.; Pecoraro, V. L.; Yano, J.; Neese, F.; DeBeer, S. The Protonation States of Oxo-Bridged Mn^{IV} Dimers Resolved by Experimental and Computational Mn K Pre-Edge X-ray Absorption Spectroscopy. *Inorg. Chem.* **2013**, *52* (22), 12904−12914.
(59) Baldwin, M. J.; Stemmler, T. L.; Riggs-Gelasco, P. J.; Kirk, M. L.; Penner-Hahn, J. E.; Pecoraro, V. L. Structural and Magnetic Effects of Successive Protonations of Oxo Bridges in High-Valent Manganese Dimers. *J. Am. Chem. Soc.* **1994**, *116* (25), 11349−11356.
(60) Niemann, A.; Bossek, U.; Wieghardt, K.; Butzlaff, C.; Trautwein, A. X.; Nuber, B. A New Structure−Magnetism Relationship for Face-Sharing Transition-Metal Complexes with d^3−d^3 Electronic Configuration. *Angew. Chem., Int. Ed. Engl.* **1992**, *31* (3), 311−313.
(61) Wieghardt, K.; Bossek, U.; Nuber, B.; Weiss, J.; Bonvoisin, J.; Corbella, M.; Vitols, S. E.; Girerd, J. J. Synthesis, crystal structures, reactivity, and magnetochemistry of a series of binuclear complexes of manganese(II), -(III), and -(IV) of biological relevance. The crystal structure of $[L'Mn^{IV}(\mu\text{-}O)_3Mn^{IV}L'](PF_6)_2\bullet H_2O$ containing an unprecedented short Mn●●●Mn distance of 2.296 Å. *J. Am. Chem. Soc.* **1988**, *110* (22), 7398−7411.
(62) Fdez. Galvan, I.; Vacher, M.; Alavi, A.; Angeli, C.; Aquilante, F.; Autschbach, J.; Bao, J. J.; Bokarev, S. I.; Bogdanov, N. A.; Carlson, R. K.; Chibotaru, L. F.; Creutzberg, J.; Dattani, N.; Delcey, M. G.; Dong, S. S.; Dreuw, A.; Freitag, L.; Frutos, L. M.; Gagliardi, L.; Gendron, F.; Giussani, A.; Gonzalez, L.; Grell, G.; Guo, M.; Hoyer, C. E.; Johansson, M.; Keller, S.; Knecht, S.; Kovacevic, G.; Kallman, E.; Li Manni, G.; Lundberg, M.; Ma, Y.; Mai, S.; Malhado, J. P.; Malmqvist, P. A.; Marquetand, P.; Mewes, S. A.; Norell, J.; Olivucci, M.; Oppel, M.; Phung, Q. M.; Pierloot, K.; Plasser, F.; Reiher, M.; Sand, A. M.; Schapiro, I.; Sharma, P.; Stein, C. J.; Sørensen, L. K.; Truhlar, D. G.; Ugandi, M.; Ungur, L.; Valentini, A.; Vancoillie, S.; Veryazov, V.; Weser, O.; Wesołowski, T. A.; Widmark, P.-O.; Wouters, S.; Zech, A.; Zobel, J. P.; Lindh, R. OpenMolcas: From Source Code to Insight. *J. Chem. Theory Comput.* **2019**, DOI: 10.1021/acs.jctc.9b00532.
(63) Keller, S.; Dolfi, M.; Troyer, M.; Reiher, M. An efficient matrix product operator representation of the quantum chemical Hamiltonian. *J. Chem. Phys.* **2015**, *143* (24), 244118.
(64) Keller, S.; Reiher, M. Spin-adapted matrix product states and operators. *J. Chem. Phys.* **2016**, *144* (13), 134101.
(65) Roos, B. O.; Lindh, R.; Malmqvist, P.-Å.; Veryazov, V.; Widmark, P.-O. Main Group Atoms and Dimers Studied with a New Relativistic ANO Basis Set. *J. Phys. Chem. A* **2004**, *108* (15), 2851−2858.
(66) Widmark, P.-O.; Malmqvist, P.-Å.; Roos, B. O. Density matrix averaged atomic natural orbital (ANO) basis sets for correlated molecular wave functions. *Theor. Chim. Acta* **1990**, *77* (5), 291−306.
(67) Reiher, M.; Wolf, A. Exact decoupling of the Dirac Hamiltonian. I. General theory. *J. Chem. Phys.* **2004**, *121* (5), 2037−2047.
(68) Reiher, M.; Wolf, A. Exact decoupling of the Dirac Hamiltonian. II. The generalized Douglas-Kroll-Hess transformation up to arbitrary order. *J. Chem. Phys.* **2004**, *121* (22), 10945−10956.
(69) Hess, B. A. Relativistic electronic-structure calculations employing a two-component no-pair formalism with external-field projection operators. *Phys. Rev. A: At., Mol., Opt. Phys.* **1986**, *33* (6), 3742−3748.
(70) Pipek, J.; Mezey, P. G. A fast intrinsic localization procedure applicable for ab initio and semiempirical linear combination of atomic orbital wave functions. *J. Chem. Phys.* **1989**, *90* (9), 4916−4926.
(71) Barcza, G.; Legeza, Ö.; Marti, K. H.; Reiher, M. Quantum-information analysis of electronic states of different molecular structures. *Phys. Rev. A: At., Mol., Opt. Phys.* **2011**, *83* (1), 012508.
(72) Fiedler, M. Algebraic connectivity of graphs. *Czechoslovak Mathematical Journal* **1973**, *23* (2), 298−305.

DOI: 10.1021/acs.jpclett.9b02417
J. Phys. Chem. Lett. 2019, 10, 6762−6770

(73) Fiedler, M. A property of eigenvectors of nonnegative symmetric matrices and its application to graph theory. *Czechoslovak Mathematical Journal* **1975**, *25* (4), 619−633.
(74) Stein, C. J.; Reiher, M. autoCAS: A Program for Fully Automated Multiconfigurational Calculations. *J. Comput. Chem.* **2019**, *40* (25), 2216−2226.

DOI: 10.1021/acs.jpclett.9b02417
J. Phys. Chem. Lett. 2019, 10, 6762−6770